Desalination and Water Treatment
www.deswater.com
doi: 10.5004/dwt.2020.26217

203 (2020) 221–229
November

Salophen functionalized hydrothermal carbon spheres for selective removal of U(VI)

You-qun Wang[a,b], De-jun Zeng[a,b], Xiao-hong Cao[a,b], Yin Dai[a,b], Hui-jie Ma[b], Yun-hai Liu[a,b,c], Zhi-bin Zhang[a,b,c,*]

[a]*State Key Laboratory of Nuclear Resources and Environment, East China University of Technology, Nanchang, Jiangxi 330013, China, emails: zhbzhang@ecut.edu.cn (Z.-b. Zhang), wangyouqun@ecit.cn (Y.-q. Wang), zengdj@ihep.ac.cn (D.-j. Zeng), 31881447@qq.com (X.-h. Cao), 94448243@qq.com (Y. Dai), walton_liu@163.com (Y.-h. Liu)*
[b]*Fundamental Science on Radioactive Geology and Exploration Technology Laboratory, East China University of Technology, Nanchang, Jiangxi 330013, China, email: 923619884@qq.com (H.-j. Ma)*
[c]*Engineering Research Center of Nuclear Technology Application (East China University of Technology), Ministry of Education, Nanchang, Jiangxi 330013, China*

Received 17 January 2020; Accepted 5 June 2020

ABSTRACT

In this work, the functional group of salophen with high affinity to U(VI) was grafted to hydrothermal carbon spheres (HCSs) to improve the adsorptive ability for U(VI). Through the application of scanning electron microscopy, Fourier transform infrared, and zeta potential measurement, the micro-morphology, functional group, and surface charge of the adsorbents was characterized. Comprehensive investigation of the factors affected U(VI) adsorbed by HCSs and salophen group modified HCSs (HCSs-sal) were conducted. Different types of kinetic and thermodynamic models were utilized to explore the adsorption processes. The results of this study, indicated that the adsorption of U(VI) on HCSs-sal fitted well to Langmuir equations with the monolayer capacity of 332.51 mg g^{-1}. Furthermore, the adsorptive selectivity of HCSs for U(VI) was also remarkably enhanced after functionalization with the salophen group. Overall, HCSs-sal appears to have the potential to be a prospective candidate for the selective adsorption of U(VI).

Keywords: Hydrothermal carbon spheres; Salophen; Adsorption; Uranium; Functionalization

1. Introduction

Due to the radioactive, accumulative, chronic, and toxic effects of U(VI) [1,2], the pollution caused by U(VI) poses a significant threat to the well-being of environment [3] in contaminated area. If U(VI) pollution left untreated, there is a heightened risk of the pollution causing severe kidney and reproductive effects as well as DNA damage [4,5]. Hence, it is urgent to discover effective techniques to separate and remove U(VI) from contaminated areas efficiently.

Adsorptive removal of U(VI) is a method with preponderances of simplicity [6], low cost [7], and high efficiency [8]. As a result, it has attracted increasing attention [9]. Using an adsorbent with a high adsorption capacity and selectivity is instrumental to the separation of U(VI) in aqueous solution. Recently, there has been widespread use of carbonaceous in the adsorption of U(VI) [5] mainly owing to their high chemical, thermal, and radiation stability [10], environmental friendly [11], and higher specific area [12], etc. HCSs, a semi-carbonaceous material, has been prepared from mono- and poly-saccharides [13,14] using

* Corresponding author.

1944-3994/1944-3986 © 2020 Desalination Publications. All rights reserved.

the hydrothermal method. In particularly, it is important to note that HCSs contains a higher oxygenated group than conventional carbon adsorbents which are calcined at high temperature [15]. By grafting various functional groups of the carboxyl [16], salicylideneimine [17], and phosphorus [6] groups have grafted to onto the surface of HCSs, it is possible to further enhance the capacity and selectivity of HCSs. However, the functional group of salophen has not reported modifying of HCSs to remove U(VI). Salophen, with four donor atoms of N and O, can easily form stable pentagonal bipyramidal coordination [18–20] with hexavalent U(VI) [4]. Owing to this, the salophen group has a critical role in determination [21] and selective separation [19,22] of U(VI) from other cations. Recently, the magnetic Schiff base (MSB) functionalized with salophen group that was prepared by Léveillé et al. [22] performed a high capacity and selectivity toward U(VI) over several metal ions.

In this study, the primary focus was on the grafting of salophen on the surface of HCSs for removing of U(VI). In addition to scanning electron microscopy (SEM) and Fourier transform infrared (FT-IR), zeta potential measurement were also applied to analyze the adsorbents. The various factors influencing adsorption of U(VI) have been optimized. The U(VI) removal processes of these two adsorbents have been investigated via various models. Furthermore, the adsorptive selectivity of HCSs-sal has been explored with a wide variety of co-existing ions.

2. Experimental

2.1. Reagents

$NaNO_2$, HCl, NaOH, and H_2O_2 were purchased from Sinopharm Chemical Reagent Co., Ltd., and were Analytical grade (AR). Moreover, the AR reagents of ethylenediamine, o-phenylenediamine, salicylide, and dicyclohexylcarbodiimide (DCC) were obtained from Aladdin reagent (Shanghai) Co., Ltd.

2.2. Synthesis of HCSs-sal

The preparation procedures of HCSs-sal are illustrated in Fig. 1. The agent of salophen was synthesized base on the methodology given in literature [23]. 1.6 g o-phenylenediamine and 3.2 mL salicylide were added in a 250 mL containing 80 mL of methanol. The mixtures were magnetically stirred at an ambient temperature for 1 h. Next, salophen was acquired once the orange precipitate collected and dried.

The preparation of HCSs and HCSs-COOH and HCSs-NH_2 were according to our previous work [24]. 0.30 g of HCSs-NH_2 was agitated for a duration of 30 min in 50 mL of 1 mol L^{-1} HCl solution under an ice bath until the powder mixed evenly. Then, the intermediate product reacted with 25 mL of 1 mol L^{-1} $NaNO_2$ at a temperature of 273.15 K for 3 h. Following centrifugalizing, and washing with deionized water till neutral, the mid-product was named as HCSs-Cl. 1.2 g of salophen was poured into 200 mL 10% NaOH and stirred for 5 h under an ice bath. Following this, 1.0 g of HCSs-Cl reacted with the alkaline salophen solution for one entire day. The products were filtered, washed, and dried in a vacuum drying oven. The final products were denoted as HCSs-sal.

2.3. Characterization

Micro-morphology of HCSs-sal was observed using a field emission SEM (NNS-450, FEI, USA). The functional groups of HCSs, HCSs-COOH, HCSs-NH_2, and HCSs-sal were analyzed via a Fourier transform infrared spectroscopy (Nexus 870, Nicolet, USA) in the wavenumbers ranging from 3,800 to 600 cm^{-1} by utilizing the method of KBr pellet. A zeta potential analyzer (Stabino, Germany) was used to record the zeta potentials of adsorbents using either diluted NaOH or HCl solution as titrant.

2.4. Adsorption

During the adsorption experiment, 10.0 mg of HCSs and HCSs-sal was mixed with 100 mL U(VI) solution at a fixed pH value in a Triangular flask. A reciprocating water bath shaker, the was used to facilitate adsorption for a specific time. The U(VI) concentrations at supernatant fraction was analyzed by the Arsenazo III-U(VI) system using a UV-Vis spectrophotometer (TU-19, Pgeneral, China) at 650 nm. An ICP-OES (Shimadzu, Japan) was applied to measure the concentration of Mg(II) and other ions. The amount of metal

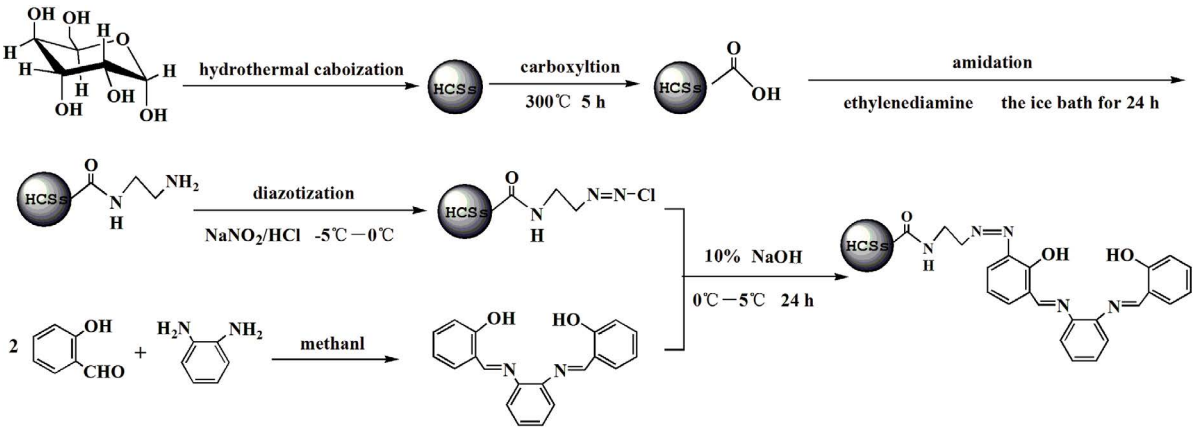

Fig. 1. Procedure diagram of the preparation of HCSs-sal.

ions adsorbed (q_e, mg g^{-1}) and the distribution coefficient (K_d, mL g^{-1}) were acquired by Eqs. (1) and (2):

$$q_e = \frac{(C_0 - C_e) \times V}{W} \quad (1)$$

$$K_d = \frac{q_e}{C_e} \times 1{,}000 \quad (2)$$

where C_0 (mg L^{-1}) and C_e (mg L^{-1}) denotes as the adsorbate concentration at beginning and equilibrium, respectively; W (g) and V (L) signifies the mass of adsorbents, and the volume of the adsorbate solution, respectively.

3. Results and discussion

3.1. Characterization

3.1.1. Scanning electron microscopy

Fig. 2 displays the SEM micrograph and the particle size distribution of HCSs-sal. It can be observed that HCSs-sal was microsphere particles in the range of 0.4–0.9 μm. It was obtained by a software of Nano Measurer 1.2. The average particle sizes were determined to be approximately 0.6 μm. The results indicated that the micro spherical geometric of HCSs has not been destructed after functionalization with the salophen group.

3.1.2. Fourier transform infrared spectroscopy

The FT-IR spectra of pristine and modified HCSs in the range of wavenumbers from 3,800 to 600 cm^{-1} (Fig. 3) were obtained by the method of KBr pellet. The broad peaks at 3,445 cm^{-1} were due to the stretching mode of O–H [25]. The peaks appearing at 1,716 and 1,622 cm^{-1} corresponded to stretching bands of C=O and C=C [26], respectively. A new peak of C–O stretching mode [27] in the carboxylic anhydride was centred at 1,257 cm^{-1} in the spectrum of HCSs-COOH, which suggested that the carboxyl group was successfully grafted to HCSs. Moreover, the three peaks at 1,674; 1,555; and 1,300 cm^{-1} could be a results of secondary amide [28], respectively. More importantly, the three peaks at 1,469; 1,054; and 680 cm^{-1} were the typical vibration peaks of benzene ring [29]. Lastly, a pair of peaks at 757 and 1,653 cm^{-1} represented C–H deformation vibration which laid outside the benzene ring surface and C=N vibration, respectively. The results implied that salophen group was successfully introduced to HCSs.

3.1.3. Zeta potential

The zeta potential values of adsorbents are illustrated in Fig. 4. It can be observed that the zero potential points of the origin HCSs and HCSs-sal was at the pH value of 2.11 and 2.46, respectively. This result indicated that the negative charge of HCSs-sal was slightly higher than that of HCSs,

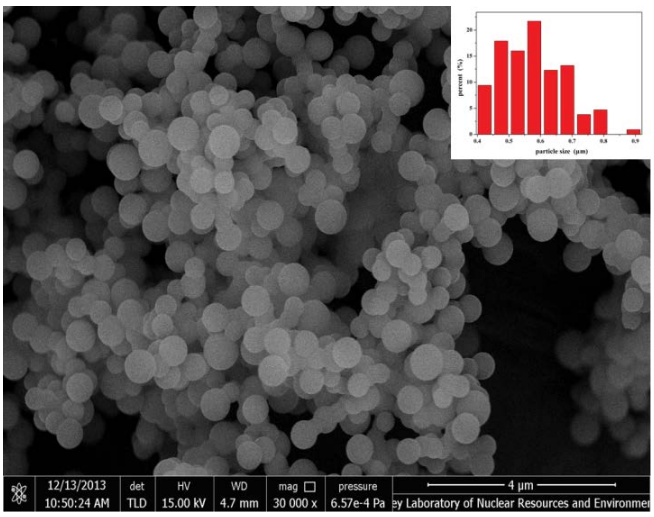

Fig. 2. SEM image of HCSs-sal (inset: particle size distribution).

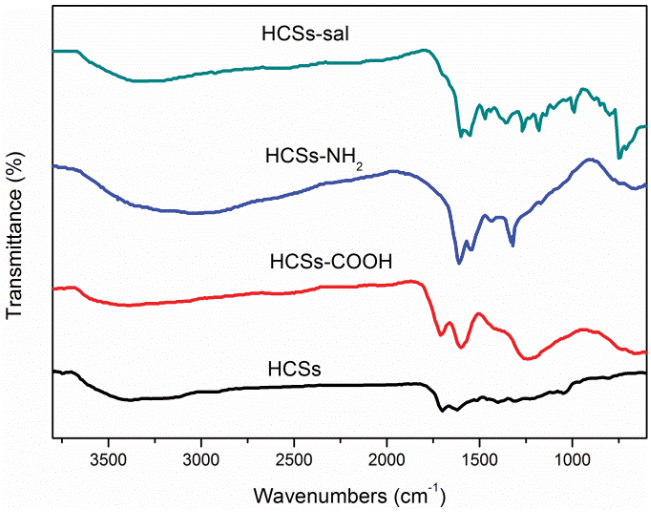

Fig. 3. FT-IR spectra for HCSs, HCSs-COOH, HCSs-NH_2, and HCSs-sal.

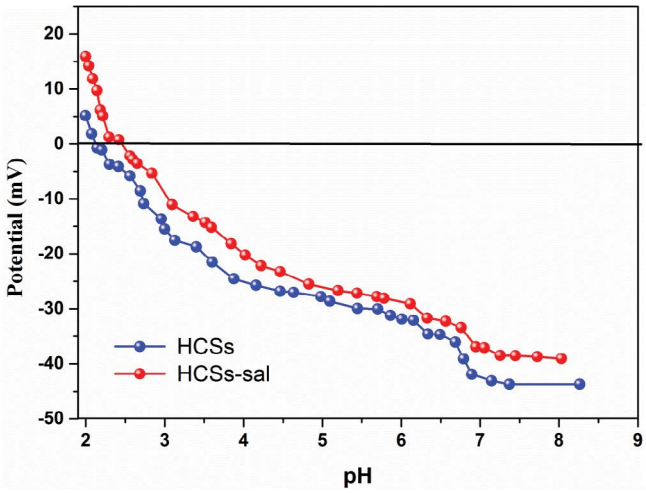

Fig. 4. Zeta potentials of HCSs and HCSs-sal at different pH values.

which can be attributed to the new emerging amine groups [30] of HCSs-sal. Moreover, the zeta potential of HCSs-sal gradually declined as the pH values increased on account of the protonation gradation of N atom in the –NH– group of HCSs-sal.

3.2. Effect of solution pH

The U(VI) ions species, their distribution, and the surface charges of adsorbents [31] are significantly affected by the pH values. The results exhibited in Fig. 5 indicate that the pHs significantly affected U(VI) uptake by HCSs and HCSs-sal.

When the solution was in an acid condition (3 ≤ pH < 6.0), the surface charges of these two adsorbents were negative (Fig. 4), and the U(VI) species were in cations form (UO_2^{2+}, $(UO_2)_2(OH)_2^{2+}$, and $(UO_2)_3(OH)_5^{+}$ [32–34]). However, the competition of a substantial quantity of H^+ or H_3O^+ with U(VI) for the surface-active sites of adsorbents led to lower adsorption amounts for U(VI) at lower pH values. In the near-neutral condition (pH 6.0), the adsorption of both HCSs and HCSs-sal maximized. The summation of $(UO_2)_3(OH)_5^{+}$ and $(UO_2)_4(OH)_7^{+}$ was around 96.7% at pH 6.0. Therefore, the electronegativity of HCSs and HCSs-sal promoted adsorbing the U(VI) by electrostatic attraction [35]. Besides, the maximum q_e of HCSs and HCSs-sal was 55.7 ± 9.0 and 281.6 ± 8.0 mg g^{-1} at the optimal pH of 6.0, respectively. Moreover, the optimal pH of 6.0 was determined by Mishra et al. [19] and Léveillé et al. [22], where the salophen was utilized as functional group to remove U(VI). At pH values higher than 7.0, the positive species of U(VI) decreased and the anion of $(UO_2)_3(OH)_7^{-}$ appeared [19]. Therefore, the electrostatic repulsion between U(VI) and negative charged HCSs and HCSs-sal resulted in the decrease of adsorption. Thus, it was deemed that the initial pH of 6.0 was optimal, and used for the subsequent experiments.

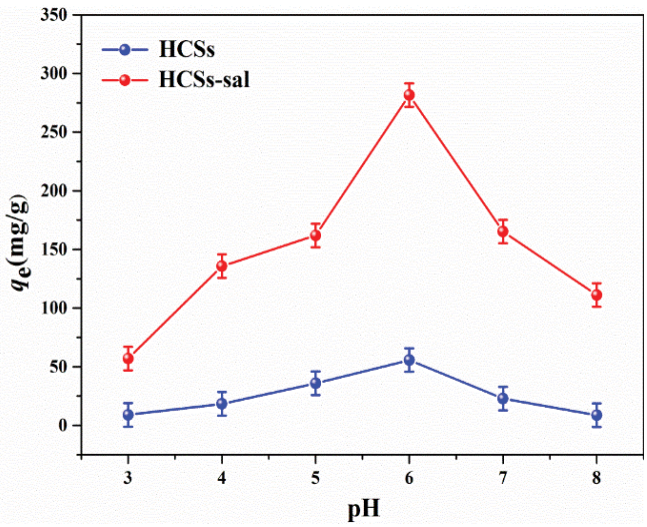

Fig. 5. Effect of pH on the U(VI) adsorption by HCSs and HCSs-sal (C_0 = 50 mg L^{-1}, V = 100 mL, T = 298.15 K, t = 180 min, and m = 10 mg).

3.3. Adsorption kinetics

Fig. 6 illustrates the U(VI) adsorption kinetics of HCSs and HCSs-sal in the in the time range from 0 to 180 min. As the contact time was extended, the amounts of U(VI) adsorbed increased gradually until it reached equilibrium within 60 min. This indicated the rapid and high efficient processes of HCSs-sal. The time to reach the equilibrium was decided as 60 min for the two adsorbents.

The pseudo-first-order [36] (PFO), pseudo-second-order [37] (PSO) kinetics, and intra particle diffusion (IPD) [38] models were applied to realize the mechanism of U(VI) removal. The expressions of the above models are listed as Eqs. (3)–(5):

$$q_t = q_e\left(1 - e^{-k_1 t}\right) \tag{3}$$

$$q_t = \frac{k_2 q_e^2 t}{1 + k q_e t} \tag{4}$$

$$q_t = k_{id} t^{0.5} \tag{5}$$

where k_1 (min^{-1}), k_2 (g mg^{-1} min^{-1}), and k_{id} (mg g^{-1} min$^{-0.5}$) denotes as the rate constant in the PFO, PSO, and IPD, respectively; q_t (mg g^{-1}) represents the quantity of U(VI) extracted in the adsorption process.

The nonlinear fitting curves of PFO and PSO are presented in Fig. 6. The parameters of $q_{e,cal}$, k_1, and k_2 are tabulated in Table 1 along with correlation coefficient(R^2). With regard to HCSs, the R^2 value of the PSO equation was calculated to be 0.955, this is extremely close to 1.0. The experimental equilibrium amount of U(VI) adsorbed by HCSs ($q_{e,exp}$ = 54.97 mg g^{-1}) was near to the calculated value (54.32 mg g^{-1}). This indicated that the adsorption of U(VI) on HCSs was explained more appropriately by the PSO model. As for HCSs-sal, the R^2 value of the two models (0.997 and 0.976) were close. Additionally, the U(VI) uptake calculated by two models (277.71 and 289.23 mg g^{-1}) were also near to

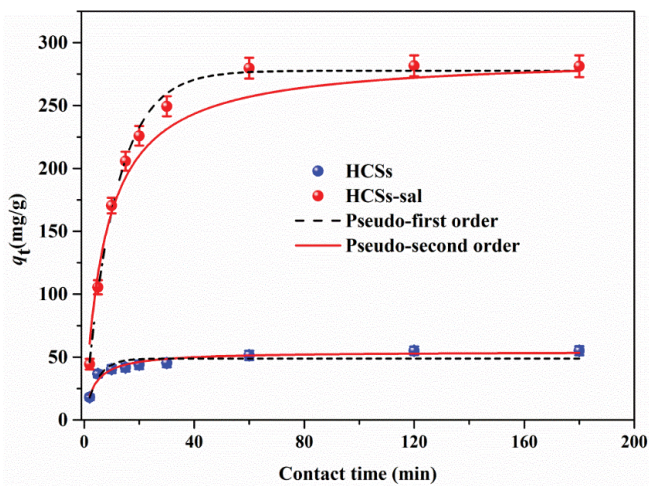

Fig. 6. Kinetics of U(VI) adsorption onto HCSs and HCSs-sal (C_0 = 50 mg L^{-1}, V = 100 mL, T = 298.15 K, pH = 6.0, and m = 10 mg).

Table 1
Kinetic parameters of U(VI) adsorption onto HCSs and HCSs- salophen

Adsorbents	$q_{e,\exp}$ (mg g^{-1})	Pseudo-first-order			Pseudo-second-order kinetics			Intra-particle diffusion		
		$q_{e,\text{cal}}$ (mg g^{-1})	k_1 (min^{-1})	R^2	$q_{e,\text{cal}}$ (mg g^{-1})	k_2 (g mg^{-1} min^{-1})	R^2	$k_{\text{id},1}$	$k_{\text{id},2}$	$k_{\text{id},3}$
HCSs	54.97	48.82	0.23	0.885	54.32	5.21×10^{-3}	0.955	22.60	2.57	0.66
HCSs-sal	283.28	277.71	0.09	0.997	289.23	4.59×10^{-4}	0.976	66.37	18.30	0.28

the actual value (283.28 mg g^{-1}). The results implied that the adsorption of U(VI) on HCSs-sal was fitted well to both PFO and PSO models, which stated that U(VI) adsorbed by HCSs-sal was principally governed by diffusion and chemical reaction [39].

In order to extensively clarify the adsorption processes, the IPD model was also adopted into investigating the kinetic data. The linear fitting plots and the values of k_{id} at different stages are given in Fig. 7 and Table 1, respectively. When analyzing the results, the U(VI) adsorption processes can be divided into three parts. The first procedure of adsorption was external surface adsorption [4] with the highest rate (22.60 and 66.37 mg g^{-1} min$^{-0.5}$). Then, the rates were gradually slower (2.57 and 18.30 mg g^{-1} min$^{-0.5}$) which was a result of the less active site on adsorbents and less U(VI) in aqueous solution. Finally, adsorptions reached equilibrium as the slope values were close to 0.

3.4. Adsorption isotherm

To better understand the adsorptive performances and mechanisms of HCSs and HCSs-sal for U(VI), isothermal curves were obtained at 298.15 K. Fig. 8 illustrates the adsorption isothermal curves, in which the amount adsorbed by the two adsorbents expanded progressively and remained unchanged as the equilibrium concentration increased.

The Langmuir [40], Freundlich [41], and Sips [38] have been commonly employed to conclusively understand the adsorption behavior. The equation of these models are displayed as Eqs. (6)–(8):

$$q_e = q_m \frac{K_L C_e}{1 + K_L C_e} \tag{6}$$

$$q_e = K_F C_e^{1/n} \tag{7}$$

$$q_e = q_{\text{ms}} \left[\frac{(K_s C_e)^{m_s}}{1 + (K_s C_e)^{m_s}} \right] \tag{8}$$

where q_m (mg g^{-1}) and q_{ms} (mg g^{-1}) presents the adsorption capacity in the Langmuir and Sips models, respectively; n and m_s are the parameters about the heterogeneity of the adsorption [4]; and K_L (L mg^{-1}), K_F (L$^{1/n}$ mg$^{1-1/n}$ g^{-1}), K_s (L mg^{-1}) m_s are the constants in these models.

Fig. 8 and Table 2 illustrate the nonlinear fitting plots and the values of the corresponding parameters along with R^2 of Langmuir, Freundlich, and Sips model according to equilibrium data of U(VI). According to the values of q_m, and q_{ms}, U(VI) adsorption on HCSs can be best described using the Sips equation better. As for HCSs-sal, the values of R^2 were 0.996 and 0.998 for Langmuir and Sips models. However, the calculated values of q_m for HCSs-sal using the Langmuir was 332.51 mg g^{-1}, which was closer to the saturated amount adsorbed (319.69 mg g^{-1}) obtained by

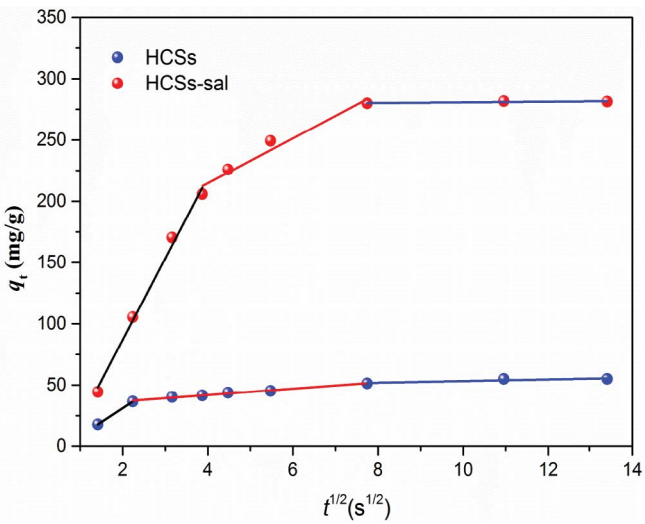

Fig. 7. Intra-particle diffusion model for the U(VI) uptake by HCSs and HCSs-sal.

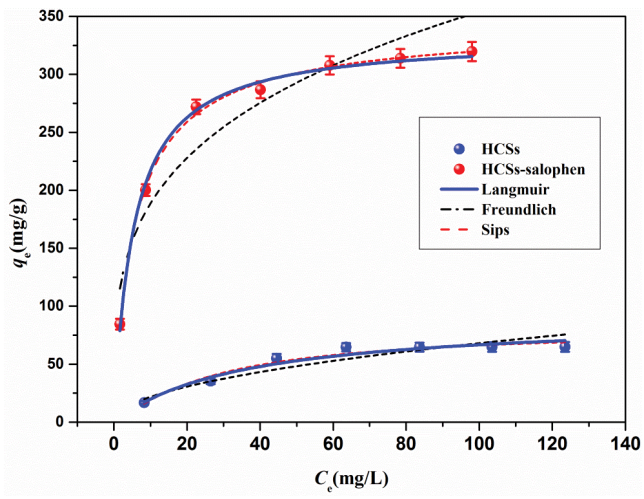

Fig. 8. Adsorption isotherm of U(VI) on HCSs and HCSs-sal (V = 100 mL, t = 120 min, T = 298.15 K, pH = 6.0, and m = 10 mg).

Table 2
Parameters of Langmuir, Freundlich, and Sips isotherm for adsorption of U(VI) onto HCSs and HCSs-sal

Adsorbents	Langmuir isotherm			Freundlich isotherm			Sips isotherm			
	q_m	K_L	R^2	K_F	n	R^2	q_{ms}	m_s	K_s	R^2
HCSs	90.50	0.02	0.973	6.92	2.04	0.919	80.51	1.17	0.04	0.971
HCSs-sal	332.51	0.20	0.996	100.41	3.70	0.904	345.06	0.90	0.17	0.998

experiments. Thus, the uptake of U(VI) on HCSs-sal can be fitted to the Langmuir equation, indicating a monolayer adsorption process. Furthermore, the adsorption capacity of HCSs was significantly improved after decoration, demonstrating a superior affinity of the salophen group to U(VI).

In addition, comparisons of HCSs-sal with the hydrothermal carbon (HTC) functionalized with the different groups in adsorption capacity for U(VI) are exhibited in Table 3. HCSs-sal (332.51 mg g^{-1}) has proven to have a an increasingly excellent adsorption capacity than the pristine HTC and HCSs or HTC. The more excellent adsorption capacity of HCSs-sal (332.51 mg g^{-1}) has proven to have an increasingly than pristine HTC and HCSs or HTC modified with carboxyl (HTC-COOH) [15], salicylideneimine (HTC-salicy) [17], catechol-like phenolic (HTC-btg), and phosphorus (HCSs-PO_4) [6] group was contributed to the high affinity of the salophen group to U(VI) [18–20].

Table 3
Comparison of HCSs-sal with other hydrothermal carbon materials in adsorption capacity

Sorbents	Experimental conditions	Capacity (mg g^{-1})	Reference
Sorbents			
(HTC)	pH = 6.0, T = 298.15 K	62.70	[15]
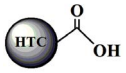 (HTC-COOH)	pH = 4.0, T = 298.15 K	205.80	[15]
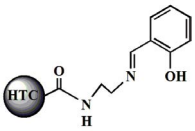 (HTC-salicy)	pH = 4.3, T = 298.15 K	261.00	[17]
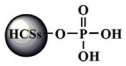 (HCSs-PO_4)	pH = 5.0, T = 298.15 K	285.70	[6]
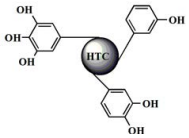 (HTC-btg)	pH = 4.5, T = 298.15 K	307.30	[42]
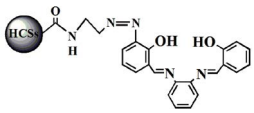 (HCSs- sal)	pH = 6.0, T = 298.15 K	332.51	This work

3.5. Adsorption thermodynamics

The values of q_e increased gradually as the temperature rose from 298.15 to 318.15 K (Fig. 9a). The results demonstrated that the adsorption was much more beneficial at a higher temperature. Different functions such as $\Delta G°$ (change of Gibbs free energy, kJ mol^{-1}), $\Delta H°$ (enthalpy, kJ mol^{-1}) as well as $\Delta S°$ (entropy of adsorption process, J K^{-1} mol^{-1}) were used to evaluate the adsorptive thermodynamics, which were obtained by Eqs. (9) and (10):

$$\ln K_d = \frac{\Delta S°}{R} - \frac{\Delta H°}{RT} \tag{9}$$

$$\Delta G° = \Delta H° - T\Delta S° \tag{10}$$

In the above equations, T (K) represents thermodynamic temperature. The computation results of $\Delta H°$ and $\Delta S°$ were obtained by the linear fitting plots in Fig. 9b.

The positive values of $\Delta H°$ and $\Delta S°$, and non-positive values of $\Delta G°$ are summarized in Table 4. The results suggested that the endothermic, randomness increasing, and spontaneous processes of U(VI) adsorption on these two adsorbents. Additionally, a higher negative value of $\Delta G°$ at 298.15 K for HCSs-sal (–22.85 kJ mol^{-1}) than HCSs (–17.56 kJ mol^{-1}), this indicated that HCSs-sal showed a higher affinity toward U(VI).

3.6. Selective study

The selective adsorption ability of HCSs-sal was also investigated in the solution containing a variety of co-existing metal cations. 0.040 g of adsorbents was added to 150 mL of simulated nuclear wastewater at the optimal pH of 6.0. The results presented in Fig. 10 indicated that q_e value of HCSs-sal for U(VI) was 36.70 mg g^{-1}, this value was at least twice as much as that of HCSs (15.19 mg g^{-1}). In addition, the Mg(II), Na(I), Mn(II), Ni(II), and Sr(II) uptake on HCSs increased after modification with the salophen group.

To compare adsorption selectivity of HCSs and HCSs-sal, the values of selectivity coefficient (S) and relative selectivity coefficient (S_r) [43] are calculated using Eqs. (11) and (12):

$$S_{UO_2^{2+}/M^{n+}} = \frac{K_d^{UO_2^{2+}}}{K_d^{M^{n+}}} \tag{11}$$

$$S_r = \frac{S_{HCSs-sal}}{S_{HCSs}} \tag{12}$$

The values of S and K_d of HCSs-sal (Table 5) values pertaining to HCSs-sal (Table 5) were significantly higher than that of HCSs. This signified the stronger affinity of salophen group to U(VI). The values of S_r were over 3.0, especially for Cs(I), Sr(II), and Na(I), this indicated the selectivity of HCSs for adsorption of U(VI) was enhanced after grafting with the salophen group.

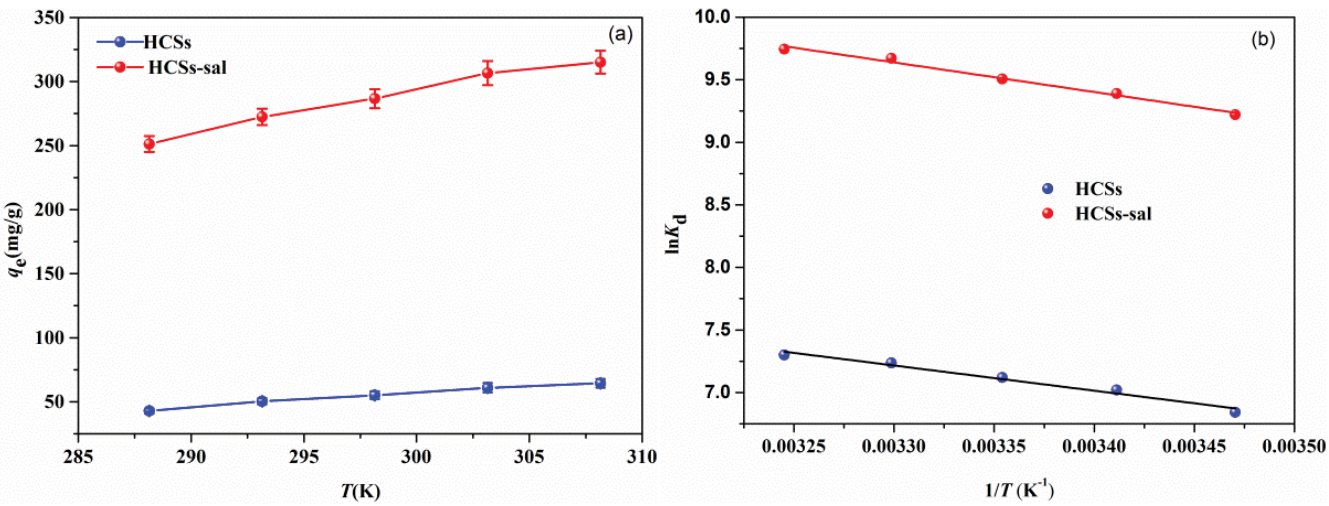

Fig. 9. (a) Effect of temperature on U(VI) adsorbed by HCSs and HCSs-sal and, (b) relationship of lnK_d with 1/T. (C_0 = 50 mg L^{-1}, t = 120 min, V = 100 mL, pH = 6.0, and m = 10 mg).

Table 4
Thermodynamic functions for adsorption of U(VI) onto HCSs and HCSs-sal

Adsorbents	$\Delta H°$ (kJ mol^{-1})	$\Delta S°$ (J K^{-1} mol^{-1})	$\Delta G°$ (kJ mol^{-1})				
			288.15 K	298.15 K	308.15 K	308.15 K	308.15 K
HCSs	16.22	115.23	–16.98	–17.56	–18.13	–18.71	–19.28
HCSs-sal	19.65	145.00	–22.13	–22.85	–23.58	–24.30	–25.03

Table 5
Distribution coefficient and selectivity coefficients of HCSs and HCSs-sal

Ions	K_d (mL g^{-1})		S		S_r
	HCSs	HCSs-sal	HCSs	HCSs-sal	
U(VI)	2,552.63	172,067.44	–	–	–
Mg(II)	159.84	225.48	15.97	763.10	47.78
Na(I)	64.87	314.27	39.35	547.52	13.91
Zn(II)	164.24	1,337.39	15.54	128.66	8.28
Mn(II)	78.81	619.25	32.39	277.86	8.58
Co(II)	85.78	894.02	29.76	192.46	6.47
Ni(II)	92.89	1,709.72	27.48	100.64	3.66
Sr(II)	195.33	717.38	13.07	239.86	18.35
Cs(I)	775.35	183.90	3.29	935.67	284.21
Hg(II)	280.04	780.97	9.12	220.32	24.17

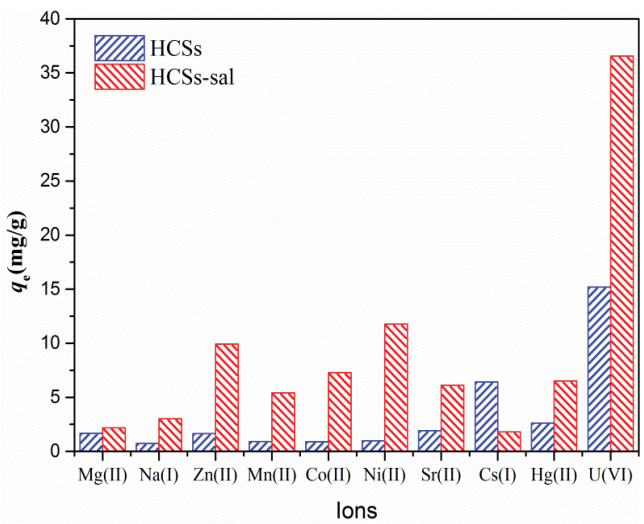

Fig. 10. Adsorption selectivity of HCSs and HCSs-sal for U(VI) with various co-existing ions (C_0 = 10 mg L^{-1}, t = 120 min, V = 150 mL, pH = 6.0, and m = 40 mg).

4. Conclusion

In conclusion, the adsorbents of HCSs functionalized with salophen group was prepared successfully. The optimal solution pHs were 6.0 for both HCSs and HCSs-sal to remove U(VI). The adsorption kinetics of HCSs-sal was rapid as it reached equilibrium within 60 min. Besides, the U(VI) adsorption process of HCSs-sal could be best fitted to PFO and PSO equations, indicating mainly controlled by the combination of diffusion and chemical reaction. Furthermore, the adsorption capacity and selectivity of HCSs were greatly enhanced, and the adsorption capacity was 332.51 mg g^{-1} once modified with the salophen group. The above results suggest that the HCSs-sal has the potential to serve as an effective material for selectively eliminating of U(VI) in wastewater.

Acknowledgments

This work was financially supported by the National Natural Science Foundation of China (21906017, 21866004, and 21866003), the Science and Technology Support Program of Jiangxi Province (Grant No. 2018ACB21007), the Jiangxi Program of Academic and Technical Leaders of Major Disciplines (Grant No. 20182BCB22011), and the Project of the Jiangxi Provincial Department of Education (Grant Nos. GJJ160550, GJJ160577). The authors declare that they have no competing interests.

References

[1] H. Pang, Z. Diao, X. Wang, Y. Ma, S. Yu, H. Zhu, Z. Chen, B. Hu, J. Chen, X. Wang, Adsorptive and reductive removal of U(VI) by Dictyophora indusiate-derived biochar supported sulfide NZVI from wastewater, Chem. Eng. J., 366 (2019) 368–377.
[2] L. Wang, H. Song, J. Li, Z. Li, Y.J. Zhang, J. Gibson, L. Zheng, Z.F. Chai, W.Q. Shi, Efficient U(VI) reduction and sequestration by Ti_2CT_x MXene, Environ. Sci. Technol., 52 (2018) 10748–10756.
[3] P. Gu, C. Zhao, T. Wen, Y. Ai, S. Zhang, W. Chen, J. Wang, B. Hu, X. Wang, Highly U(VI) immobilization on polyvinyl pyrrolidine intercalated molybdenum disulfide: experimental and computational studies, Chem. Eng. J., 359 (2019) 1563–1572.
[4] L. Yin, Y. Hu, R. Ma, T. Wen, X. Wang, B. Hu, Z. Yu, T. Hayat, A. Alsaedi, X. Wang, Smart construction of mesoporous carbon templated hierarchical Mg–Al and Ni–Al layered double hydroxides for remarkably enhanced U(VI) management, Chem. Eng. J., 359 (2019) 1550–1562.
[5] D. Plaire, J.P. Bourdineaud, A. Alonzo, V. Camilleri, L.G. Sanchez, C.A. Guillermin, F. Alonzo, Transmission of DNA damage and increasing reprotoxic effects over two generations of *Daphnia magna* exposed to uranium, Comp. Biochem. Physiol. C: Pharmacol. Toxicol., 158 (2013) 231–243.
[6] Z.B. Zhang, Z.W. Zhou, X.H. Cao, Y.H. Liu, G.X. Xiong, P. Liang, Removal of uranium(VI) from aqueous solutions by new phosphorus-containing carbon spheres synthesized via one-step hydrothermal carbonization of glucose in the presence of phosphoric acid, J. Radioanal. Nucl. Chem., 299 (2014) 1479–1487.
[7] R.A. Shawabkeh, D.A. Rockstraw, R.K. Bhada, Copper and strontium adsorption by a novel carbon material manufactured from pecan shells, Carbon, 40 (2002) 781–786.
[8] L. Tan, X. Zhang, Q. Liu, J. Wang, Y. Sun, X. Jing, J. Liu, D. Song, L. Liu, Preparation of magnetic core–shell iron oxide@silica@nickel-ethylene glycol microspheres for highly efficient sorption of uranium(vi), Dalton Trans., 44 (2015) 6909–6917.
[9] H. Heshmati, M.T. Mostaedi, H.G. Gilani, A. Heydari, Kinetic, isotherm, and thermodynamic investigations of uranium(VI) adsorption on synthesized ion-exchange chelating resin and prediction with an artificial neural network, Desal. Water. Treat., 55 (2015) 1076–1087.
[10] Y.H. Liu, Z.B. Zhang, Z.W. Zhou, G.X. Xiong, X.H. Cao, Removal of thorium(IV) from aqueous solutions by carboxyl-rich hydrothermal carbon spheres through low-temperature heat treatment in air, Desal. Water Treat., 54 (2015) 2516–2529.
[11] X. Zhang, J. Wang, R. Li, Q. Liu, L. Li, J. Yu, M. Zhang, L. Liu, Efficient removal of uranium(VI) from aqueous systems by heat-treated carbon microspheres, Environ. Sci. Pollut. Res., 20 (2013) 8202–8209.
[12] S.M. Yakout, Evaluation of mineral and organic acids on the selective separation of radioactive elements (U and Th) using modified carbon, Desal. Water. Treat., 57(2016) 3292–3297.
[13] X. Sun, Y. Li, Colloidal carbon spheres and their core/shell structures with noble-metal nanoparticles, Angew. Chem. Int. Ed., 116 (2004) 607–611.
[14] Q. Wang, H. Li, L. Chen, X. Huang, Monodispersed hard carbon spherules with uniform nanopores, Carbon, 39 (2001) 2211–2214.

[15] Z.B. Zhang, X.H. Cao, P. Liang, Y.H. Liu, Adsorption of uranium from aqueous solution using biochar produced by hydrothermal carbonization, J. Radioanal. Nucl. Chem., 295 (2013) 1201–1208.
[16] B. Han, E. Zhang, G. Cheng, L. Zhang, D. Wang, X. Wang, Hydrothermal carbon superstructures enriched with carboxyl groups for highly efficient uranium removal, Chem. Eng. J., 338 (2018) 734–744.
[17] W. Hang, L. Ma, K. Cao, J. Geng, J. Liu, S. Qiang, X. Yang, S. Li, Selective solid-phase extraction of uranium by salicylideneimine-functionalized hydrothermal carbon, J. Hazard. Mater., 229–230 (2012) 321–330.
[18] M. Yang, L. Liao, G. Zhang, B. He, X. Xiao, Y. Lin, C. Nie, Detection of uranium with a wireless sensing method by using salophen as receptor and magnetic nanoparticles as signal-amplifying tags, J. Radioanal. Nucl. Chem., 298 (2013) 1393–1399.
[19] S. Mishra, J. Dwivedi, A. Kumar, N. Sankararamakrishnan, Studies on salophen anchored micro/meso porous activated carbon fibres for the removal and recovery of uranium, RSC Adv., 5 (2015) 33023–33036.
[20] I. Liatsou, I. Pashalidis, A. Nicolaides, Triggering selective uranium separation from aqueous solutions by using salophen-modified biochar fibers, J. Radioanal. Nucl. Chem., 318 (2018) 2199–2203.
[21] M. Wu, L. Liao, M. Zhao, Y. Lin, X. Xiao, C. Nie, Separation and determination of trace uranium using a double-receptor sandwich supramolecule method based on immobilized salophen and fluorescence labeled oligonucleotide, Anal. Chim. Acta, 729 (2012) 80–84.
[22] L.W. Léveillé, N. Reynier, D. Larivière, Selective removal of uranium from rare earth leachates via magnetic solid-phase extraction using Schiff base ligands, Ind. Eng. Chem. Res., 58 (2019) 306–315.
[23] G. Zhang, L. Liao, Y. Lin, M. Yang, C. Nie, Determination of fructose 1,6-bisphosphate using a double-receptor sandwich type fluorescence sensing method based on uranyl–salophen complexes, Anal. Chim. Acta, 784 (2013) 47–52.
[24] Z.J. Lai, Z.B. Zhang, X.H. Cao, Y. Dai, R. Hua, Z.G. Le, M.B. Luo, Y.H. Liu, Synthesis of novel functional hydrothermal carbon spheres for removal of uranium from aqueous solution, J. Radioanal. Nucl. Chem., 310 (2016) 1335–1344.
[25] P.E. Fanning, M.A. Vannice, A DRIFTS study of the formation of surface groups on carbon by oxidation, Carbon, 31 (1993) 721–730.
[26] S. Li, Ag@C core/shell structured nanoparticles: controlled synthesis, characterization, and assembly, Langmuir, 21 (2005) 6019–6024.
[27] Z. Chen, L. Ma, S. Li, J. Geng, Q. Song, J. Liu, C. Wang, H. Wang, J. Li, Z. Qin, S. Li, Simple approach to carboxyl-rich materials through low-temperature heat treatment of hydrothermal carbon in air, Appl. Surf. Sci., 257 (2011) 8686–8691.
[28] O. Cozar, N. Leopold, C. Jelic, V. Chiş, L. David, A. Mocanu, M. Tomoaia-Cotişel, IR, Raman and surface-enhanced Raman study of desferrioxamine B and its Fe(III) complex, ferrioxamine B, J. Mol. Struct., 788 (2006) 1–6.
[29] J. Zhu, G. Zhang, J. Li, Z. Fang, Synthesis, adsorption and dispersion of a dispersant based on starch for coal–water slurry, Colloids Surf., A, 422 (2013) 165–171.
[30] J. Xu, L. Zhou, Y. Jia, Z. Liu, A.A. Adesina, Adsorption of thorium(IV) ions from aqueous solution by magnetic chitosan resins modified with triethylene-tetramine, J. Radioanal. Nucl. Chem., 303 (2015) 347–356.
[31] Z.B. Zhang, Y.H. Liu, X.H. Cao, P. Liang, Sorption study of uranium on carbon spheres hydrothermal synthesized with glucose from aqueous solution, J. Radioanal. Nucl. Chem., 295 (2013) 1775–1782.
[32] L. Yin, B. Hu, L. Zhuang, D. Fu, J. Li, T. Hayat, A. Alsaedi, X. Wang, Synthesis of flexible cross-linked cryptomelane-type manganese oxide nanowire membranes and their application for U(VI) and Eu(III) elimination from solutions, Chem. Eng. J., 381 (2020) 122744, https://doi.org/10.1016/j.cej.2019.122744.
[33] Y.Q. Wang, Z.B. Zhang, Y.H. Liu, X.H. Cao, Y.T. Liu, Q. Li, Adsorption of U(VI) from aqueous solution by the carboxyl-mesoporous carbon, Chem. Eng. J., 198–199 (2012) 246–253.
[34] S. Yang, Q. Li, L. Chen, Z. Chen, B. Hu, H. Wang, X. Wang, Synergistic removal and reduction of U(VI) and Cr(VI) by Fe_3S_4 micro-crystal, Chem. Eng. J., 385 (2020) 123909, https://doi.org/10.1016/j.cej.2019.123909.
[35] M. Chaudhary, L. Singh, P. Rekha, V.C. Srivastava, P. Mohanty, Adsorption of uranium from aqueous solution as well as seawater conditions by nitrogen-enriched nanoporous polytriazine, Chem. Eng. J., 378 (2019) 122236, https://doi.org/10.1016/j.cej.2019.122236.
[36] Z.J. Yi, J. Yao, Kinetic and equilibrium study of uranium(VI) adsorption by *Bacillus licheniformis*, J. Radioanal. Nucl. Chem., 293 (2012) 907–914.
[37] G. Tian, J. Geng, Y. Jin, C. Wang, S. Li, Z. Chen, H. Wang, Y. Zhao, S. Li, Sorption of uranium(VI) using oxime-grafted ordered mesoporous carbon CMK-5, J. Hazard. Mater., 190 (2011) 442–450.
[38] Y. Wang, Z. Gu, J. Yang, J. Liao, Y. Yang, N. Liu, J. Tang, Amidoxime-grafted multiwalled carbon nanotubes by plasma techniques for efficient removal of uranium(VI), Appl. Surf. Sci., 320 (2014) 10–20.
[39] L. Chen, Y.Y. Zhu, H.Q. Luo, J.Y. Yang, Characteristic of adsorption, desorption, and co-transport of vanadium on humic acid colloid, Ecotoxicol. Environ. Saf., 190 (2020) 110087, https://doi.org/10.1016/j.ecoenv.2019.110087.
[40] I. Langmuir, The constitution and fundamental properties of solids and liquids, J. Am. Chem. Soc., 38 (1917) 2221–2295.
[41] H.F.M. Freundlich, Über die adsorption in lösungen, Z. Phys. Chem., 57 (1906) 115–124.
[42] B. Li, L. Ma, Y. Tian, X. Yang, J. Li, C. Bai, X. Yang, S. Zhang, S. Li, Y. Jin, A catechol-like phenolic ligand-functionalized hydrothermal carbon: one-pot synthesis, characterization and sorption behavior toward uranium, J. Hazard. Mater., 271 (2014) 41–49.
[43] Y. Liu, X. Cao, R. Hua, Y. Wang, Y. Liu, C. Pang, Y. Wang, Selective adsorption of uranyl ion on ion-imprinted chitosan/PVA cross-linked hydrogel, Hydrometallurgy, 104 (2010) 150–155.